https://doi.org/10.5194/hess-2022-12
Preprint. Discussion started: 1 February 2022

Hydrology and Earth System Sciences
Discussions

In-situ estimation of soil hydraulic and hydrodispersive properties by inversion of Electromagnetic Induction measurements and soil hydrological modeling

Giovanna Dragonetti[1,Ψ], Mohammad Farzamian[2,3,Ψ], Antonio Coppola[4], Angelo Basile[5], Fernando Monteiro Santos[4]

[1]Mediterranean Agronomic Institute of Bari, Valenzano (BA), 70010, Italy

2Instituto Nacional de Investigação Agrária e Veterinária, Oeiras, 2780-157, Portugal

[3]Instituto Dom Luiz, Faculdade de Ciências da Universidade de Lisboa, Lisboa, 1749-016, Portugal

[4]Institute for Mediterranean Agricultural and Forestry Systems, National Research Council, Portici (NA), 80055, Italy

[5]School of Agricultural, Forestry, Food and Environmental Sciences, University of Basilicata, Potenza, 85100, Italy

Ψ These authors contributed equally to this work.

Correspondence: Mohammad Farzamian (mohammad.farzamian@iniav.pt) and Giovanna Dragonetti (dragonetti@iamb.it)

Abstract

Determining soil hydraulic and hydrodispersive properties is crucial for the sustainable management of water resources and agricultural land. Due to the local heterogeneity of soil hydrological properties and the lack of fast in-situ measurement techniques, it is hard to assess these properties at the field scale. The present study proposes a methodology based on the integration of Electromagnetic Induction (EMI) and hydrological modeling to estimate soil hydraulic and transport properties at the field scale.

To this aim, two sequential water infiltration and solute transport experiments were carried out over a small field plot. The propagation of wetting front and solute concentration along the soil

https://doi.org/10.5194/hess-2022-12
Preprint. Discussion started: 1 February 2022

profile was monitored using an EMI sensor (i.e. CMD mini-Explorer), Time Domain Reflectometry (TDR) probes, and tensiometers. Time-lapse apparent electrical conductivity (σ_a) data obtained from the EMI sensor were inverted to estimate the evolution of the vertical distribution of the bulk electrical conductivity (σ_b) over time. The σ_b distributions were converted to water content and solute concentration by using a laboratory calibration, relating σ_b to water content (θ) and soil solution electrical conductivity (σ_w). The hydraulic and hydrodispersive properties were then obtained by an optimization procedure minimizing the deviations between the numerical solution of the water flow and solute transport processes and the estimated water contents and concentrations inferred from the EMI results. The EMI-based results were finally compared to the results obtained from the in-situ TDR and tensiometer measurements.

In general, the EMI readings lead to underestimated water contents as compared to the TDR data. And yet, the water content changes over time detected by the EMI closely followed those observed by TDR and contain enough information for effective EMI-based reconstructions of water retention and hydraulic conductivity curves for the soil profile. In addition, this allowed us to reproduce the solute concentration distributions and thus the hydro-dispersive properties of the soil profile. Overall, the results suggest that time-lapse EMI measurements could be used as a rapid, non-invasive, field-scale method to assess soil hydraulic and hydro-dispersive properties, which are critical to hydrological models for agro-environmental applications.

https://doi.org/10.5194/hess-2022-12
Preprint. Discussion started: 1 February 2022

1. INTRODUCTION

Irrigated agriculture plays a crucial role in the food supply in many countries where ecological conditions are characterized by warm and dry summers with high solar radiation and evapotranspiration rates. Evaluating spatio-temporal variability of soil water and solute content is critical for optimal irrigation scheduling in timing, quantity, and quality (Coppola et al., 2019) and soil salinization assessment which depends on the variability of soil hydrological behavior (Chaali et al., 2013; Coppola et al., 2015). Soil hydrological behavior is generally described by solving the Richards' equation (RE) for water flow and the Advective-Dispersive equation (ADE) for solute transport, which is frequently assumed to apply at different spatial scales, from laboratory to field to larger scales (Sposito, 1998). These equations require the soil water retention and the soil hydraulic conductivity functions, as well as the hydro-dispersive properties, to be known at the scale of concern (Basile et al., 2003, 2006; Zech et al., 2015). Thus, the measurement methods and, consequently, the volumes investigated must be able to capture the hydraulic functions and dispersivity at the appropriate scale.

Yet, laboratory-scale measurements of hydraulic properties and dispersivity have been frequently used for field-scale studies (Coppola et al., 2011a; Comegna et al., 2012). However, one has to be aware that the validity of these lab-based properties for solving RE and ADE at field scale is essentially related to the size of the volume investigated, which has to appropriately represent the heterogeneity of the medium being studied (Wessolek et al., 1994; Ellsworth et al., 1996; van Genuchten et al., 1999; Inoue et al., 2000; Basile et al., 2003, 2006). An additional concern in lab-scale measurements is determining the hydrological properties of different soil horizons separately and then combining these properties to determine the behavior of the entire soil profile. This is especially important in the case of solute transport, where the transport process

https://doi.org/10.5194/hess-2022-12
Preprint. Discussion started: 1 February 2022

may change significantly depending on the solute travel times correlation among different layers (Coppola et al., 2011b).

In situ methods also provide the proper properties to solve RE and ADE at the field scale. In situ methods typically evaluate soil hydrological properties by monitoring infiltration and/or redistribution water flow processes, and hydro-dispersive parameters by monitoring mixing processes following pulse or step inputs of a tracer on a large plot or a long field transect (Severino et al., 2010; Coppola et al., 2011b). Inverse modeling is then frequently used to estimate the hydraulic and transport parameters simultaneously (Abbasi et al., 2003; Groh et al., 2018). Tension infiltrometers are also commonly used to monitor infiltration processes in situ for inverse-modeling of parameters (Simunek et al., 1998; Coppola et al., 2011a; Wang et al., 2013); however, the measurement volume is too small to accurately characterize the behavior of a whole soil profile. Thus, in general, for larger scale studies, in situ methods looking at the whole soil profile are generally desirable. Yet, where a large number of field locations have to be characterized, all the in-situ methods remain extremely difficult to implement and it remains critical to finding alternative methods of characterization of soil hydrology, which are fast enough and actually represent the in-situ behavior of the soil.

Geophysical methods such as the electrical resistivity tomography (ERT) technique are used as a promising alternative to traditional techniques for soil hydraulic and transport parameters assessment. Many researchers have used the time-lapse ERT data (Binley et al., 2002; Kemna et al., 2002; Singha and Gorelick, 2005; Farzamian et al., 2015a) to monitor temporal water content and solute concentration changes for the estimation of soil hydraulic and transport properties in flow and transport models. The electrical conductivity of any subsurface material is a complex function of different soil properties such as soil texture (Farzamian et al., 2020). However, the dependence of variations of soil electrical conductivity on changes in soil water content and concentration is the key mechanism that permits the use of time-lapse ERT to monitor water and solute movement in time-lapse mode through empirical or semi-empirical relationships (e.g. Archie, 1942) or established in-situ relationships (e.g. Binley et al., 2002; Farzamian et al. 2017). While this method is still widely used for soil hydraulic parameters assessment, the efficiency of this method is limited in the root-zone investigation on a field scale, given the large number of electrodes that need to be installed for shallow investigation.

To improve soil electrical conductivity surveying over large areas and within the root zone for agricultural and environmental applications, electromagnetic induction (EMI) can be used as an alternative to the ERT technique as it allows for rapid survey at a relatively low cost for shallow investigation. Apparent electrical conductivity (σ_a) data, obtained from EMI sensors at field-scale has been used to map the geospatial and temporal variability of the soil water content and salinity (Corwin and Lesch, 2005; Bouksila et al. 2012; Coppola et al., 2016; Saeed et al., 2017). However, the usefulness of σ_a is limited when studying the variation of the soil parameters with depth, as σ_a is a depth-weighted, average conductivity measurement and does not represent the soil bulk electrical conductivity (σ_b) distribution with depth (Farzamian et al., 2019).

More recently, technological advances have seen the development of multi-coil EM sensors which are designed to collect σ_a at multiple coil spacing and orientations simultaneously in one pass. This allows a rapid investigation of the soil's electrical conductivity at several depth ranges. In addition, several inversion methods have been proposed to obtain the distribution of the σ_b from σ_a measurements (Monteiro Santos, 2004; Farzamian et al., 2015b; Moghadas et al., 2019; Zare et al. 2020; Mclachlan et al. 2020). The EMI survey and inversion algorithm has now led to significant improvement in soil digital mapping and equipped soil scientists with a field-scale and cost-effective technology to obtain soil moisture and salinity (Koganti et al., 2018; Dragonetti et al., 2018; Farzamian et al., 2019; Paz et al., 2019; 2020a) with depth over large areas quickly and cheaply. Most recently, time-lapse EMI surveys and inversion modeling have been also used to study the dynamic of water content (Huang et al., 2016; Whalley et al., 2017) and soil salinity (Paz et al. 2020b; Farzamian et al. 2021). However, the potential of this method in assessing soil hydraulic and hydro-dispersive parameters has not been yet studied due to the lack of high-resolution and well-controlled experiments, required to catch the complexity of water flow and transport process during infiltration events.

With these premises, we propose a procedure based on a sequence of water infiltration and solute transport experiments, both monitored by an EMI sensor, with the objective of estimating field soil hydraulic and solute dispersivity parameters with a non-invasive sensor and relatively short field experiments. The sequence of water and solute infiltration has the main aim to discriminate the contribution of the water content and the soil solution electrical conductivity to the EMI-based σ_b. This issue will be clarified in detail in the Hydro-Geophysical approach section. The goodness of these parameter estimations will be evaluated by comparing the EMI-based hydraulic and hydrodispersive properties to those obtained from in-situ TDR and tensiometer measurements.

2. Hydro-geophysical approach

A six-step procedure, schematized in Fig. 1, was taken in order to investigate the potential of the EMI method in estimating the soil hydraulic and hydro-dispersive properties: 1) inversion of time-lapse σ_a data obtained during two experiments to generate EMI-based σ_b distributions for each experiment; 2) laboratory calibration of θ-σ_b-σ_w in order to convert σ_b distributions to water content (first experiment) and solute concentrations, [Cl^-], (second experiment); 3) converting σ_b

https://doi.org/10.5194/hess-2022-12
Preprint. Discussion started: 1 February 2022

distributions obtained from the first experiment to as many water content distributions, to be used in the next step; 4) numerical simulation (by using the HYDRUS-1D model) of the first water infiltration process in order to estimate the van Genuchten-Mualem model (vG-M) parameters through an inversion procedure based on the water contents inferred from step 3; 5) converting σ_b distributions inferred from the second experiment to $[Cl^-]$ distribution in order to estimate longitudinal dispersivity. In this step, the soil solution electrical conductivity (σ_w) distribution was estimated by using the laboratory θ-σ_b-σ_w calibration. The θ distribution in the second experiment was simulated based on the vG-M parameters obtained in step 4. This is a crucial step in the proposed procedure, as this allows to discriminate the contribution of the soil water electrical conductivity to the EMI-based σ_b. The σ_w distributions were thus converted to $[Cl^-]$ by a calibration σ_w-$[Cl^-]$; 6) numerical simulation of the second solute infiltration process in order to estimate dispersivity through an inversion procedure based on the concentrations coming from step 5.

An alternative dataset of θ and σ_b obtained from direct TDR measurements, as well as tensiometer pressure head (h) readings, collected during the two experiments, allowed us to obtain independent hydraulic and hydrodispersive properties to be used as a reference to evaluate the EMI-based parameter estimation.

https://doi.org/10.5194/hess-2022-12
Preprint. Discussion started: 1 February 2022

Hydrology and Earth System Sciences
Discussions

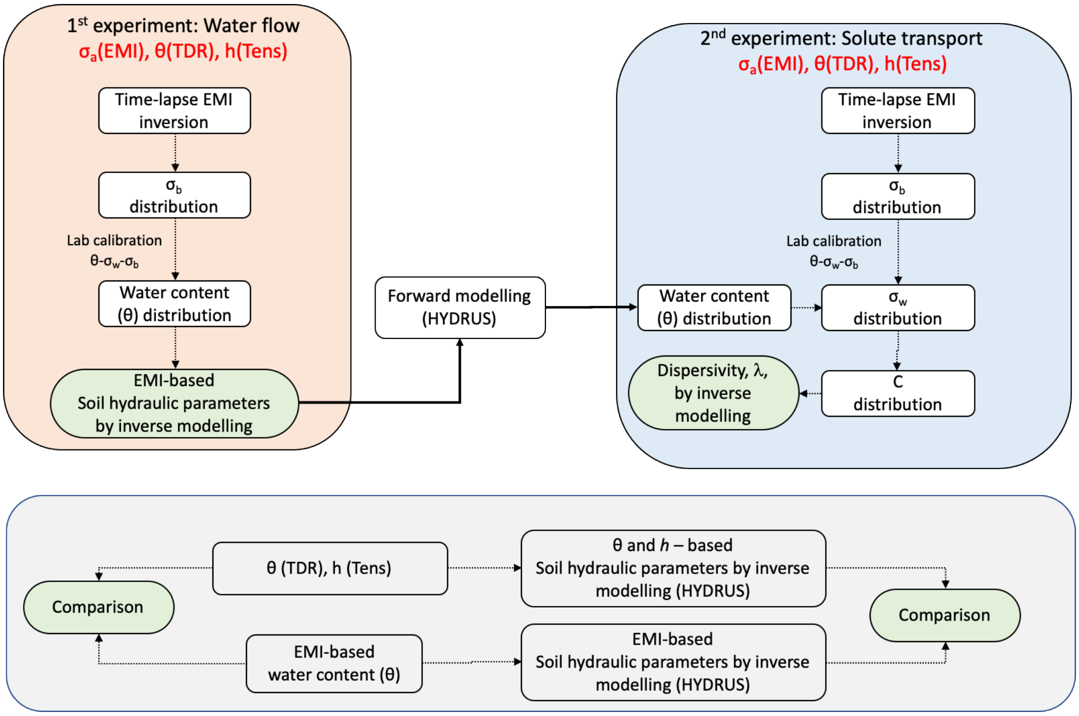

Figure 1: Schematic diagram of the proposed Hydro-Geophysical approach

3. MATERIAL AND METHODS

3.1. Study area

The experiment was performed at the Mediterranean Agronomic Institute of Bari (CIHEAM-IAM), south-eastern coast of Italy. The study area is located at an altitude of 72 m with 41° 3' 13.251" N, the longitude of 16° 52' 36.274" E, and elevation of about 68 m a.s.l. with a typical Mediterranean climate with rainy winters and very hot dry summers. The soil is a Colluvic Regosol consisting of silty loam layers of an average depth of 70 cm on a shallow fractured calcareous rock. The soil is frequently tilled at 25-30 cm, and scattered calcareous fragments are present due to the frequent breaking and grinding of the bedrock using heavy machinery to improve the soil structure and increase soil depth for plantation.

3.2. Experimental set-up

A layout of the experimental setup is shown in Fig. 2. The plot sizes 4 × 4 m. Water was applied by using a drip irrigation system consisting of 20 lines, with drippers spaced 0.20 m and delivering a nominal flow rate of 10 l h^{-1}. The drip irrigation system was placed on a metallic grid to be easily moved away from the plot and whenever EMI measurements were taken on the ground soil. The experimental plot was covered with a plastic sheet about four months prior to the experiment to keep the experimental plot under dry and a uniform water content condition at the beginning of the experiment.

Prior to the water infiltration experiments, eight three-wire TDR probes, 7 cm long, 2.5 cm internal distance, and 0.3 cm in diameter, were inserted horizontally at 2 depths − 20 and 40 cm, corresponding to the Ap and the Bw horizon − in the 4 corners of the experimental plot (at 1 m distance from the plot edge), as shown in Fig. 2. A Tektronix 1502C cable tester (Tektronix Inc., Baverton, OR) was used in this study, enabling simultaneous measurement of water content, θ, and bulk electrical conductivity, σ_b, of the soil volume explored by the probe (Robinson et al., 2003; Coppola et al., 2011a, b; 2013). Furthermore, eight tensiometers were vertically inserted near each TDR probe to acquire water potentials by a Tensicorder sensor (Hydrosense3 SK800). The experimental plot was firstly irrigated by using tap water with an electrical conductivity of about 1 dS m^{-1}. Eleven irrigation supplies were applied at regular intervals during one day at a 1 h frequency. Overall, an average water volume of 2000 l was supplied.

https://doi.org/10.5194/hess-2022-12
Preprint. Discussion started: 1 February 2022

The propagation of the wetting front along the soil profile was monitored by using an EMI sensor (i.e. CMD mini-Explorer, GF Instruments, Czech Republic), positioned horizontally in the middle of the plot (see Fig. 2) in order to measure the apparent electrical conductivity, σ_a, in the soil profile in VCP (vertical coplanar, i.e., horizontal magnetic dipole configuration) mode and then HCP (horizontal coplanar, i.e., vertical magnetic dipole configurations) mode by rotating the probe 90° axially to change the orientation from VCP to HCP mode. The CMD Mini-Explorer operates at 30 kHz frequency and has three receiver coils with 0.32, 0.71 and 1.18 m distances from the transmitter coil, referred to hereafter as ρ32, ρ71, and ρ118. The manufacturer indicates that the instrument has an effective depth range of 0.5, 1.0 and 1.8 m in the HCP mode, which is reduced to half (0.25, 0.5, and 0.9 m) by using the VCP orientation. As a consequence, this EMI sensor returns six different σ_a values (utilizing three offsets with two coil orientations) with each corresponding to different depth sensitivity ranges. All measurements were performed five minutes after each water pulse application by temporarily removing the irrigation grid. The infiltration was also monitored by TDR probes and tensiometers in order to monitor the space-time evolution of water content, θ, pressure head, h, as well as bulk electrical conductivity, σ_b. The distance of the TDR probes and tensiometers to the middle of the plot was specifically designed to avoid any interference with the EMI measurements.

https://doi.org/10.5194/hess-2022-12
Preprint. Discussion started: 1 February 2022

Hydrology and Earth System Sciences
Open Access
Discussions

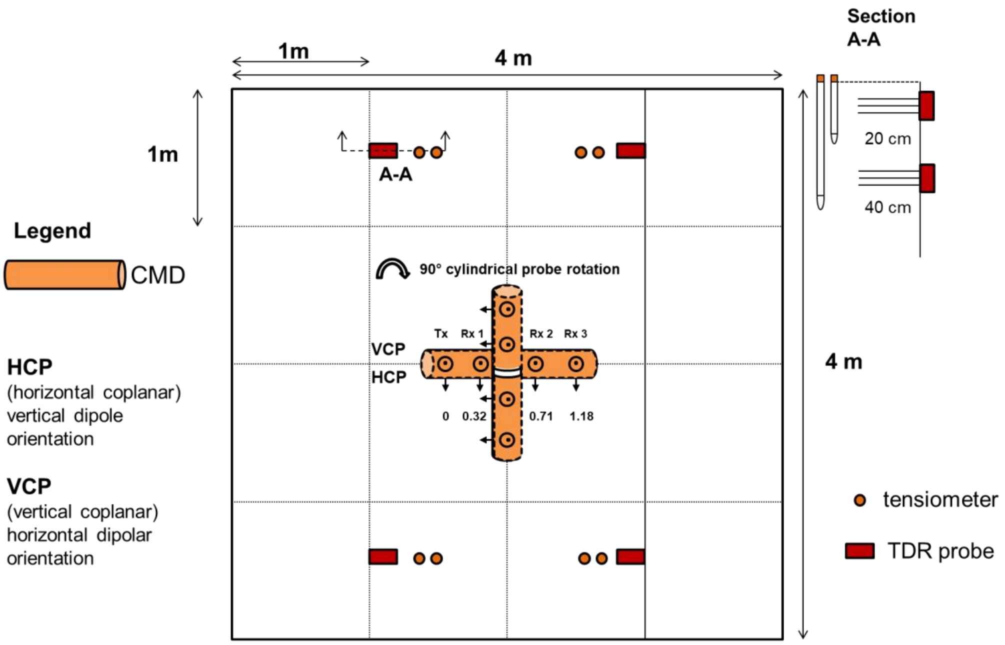

Figure 2. Layout of the experimental and monitoring set-up

At the end of the 1st water infiltration experiment, the soil was allowed to dry again (by drainage and evaporation) to bring the distribution of water content along the profile similar to the initial one (observed before the water infiltration test). Afterward, a similar infiltration experiment (2nd) was carried out but using saline water at an electrical conductivity of 15 dS m^{-1}, and obtained by mixing $CaCl_2$ into the tap water. Again, eleven saline water supplies were provided at intervals of 1h apart. In the 1st experiment, an average saline water volume of 2000 liters was supplied for all irrigation events. The propagation of the water and chloride during the 2nd infiltration experiment was monitored similarly to the 1st experiment using TDR probes, tensiometers, and the CMD Mini-Explorer sensor.

3.3. Site-specific calibration θ-σ_w-σ_b

The relationship among bulk electrical conductivity (σ_b), the electrical conductivity of the soil solution soil water (σ_w) and the water content were obtained by using the model proposed by Malicki and Walczak, (1999):

$$\sigma_w = \frac{\sigma_b - a}{(\varepsilon_b - b)(0.0057 + 0.000071S)}, \tag{1}$$

where ε_b (-) is the dielectric constant, which is related to the water content. The parameters a = 3.6 d Sm^{-1}; b = 0.11 were obtained in a laboratory experiment reported in Farzamian et al. (2021). An additional linear calibration, obtained by using solutions at different concentrations of calcium chloride was used to relate soil water concentrations, Cl^-, to σ_w.

3.4. Forward modeling and time-lapse inversion of EMI σ_a data

Time-lapse (TL) σ_a data obtained during the experiments were inverted using a modified inversion algorithm proposed by Monteiro Santos et al. (2004) to obtain σ_b distribution in time. The aim of the inversion is to minimize the penalty function that consists of a combination between the observations' misfit and the model roughness (Farzamian et al., 2019). The earth model used in the inversion process consists of a set of 1D models distributed according to the number of time-lapse measurements. All the models have the same number of layers (7) whose thickness is kept constant. The parameters of each model are spatially and temporally constrained using their neighbors through smooth conditions. The forward modeling is solved based on the full solution of the Maxwell equations (Kaufman and Keller, 1983) to calculate the σ_a responses of the model. The TL inversion algorithm is Occam-regularization and the objective function was developed based on Sasaki, (2001). Therefore, the corrections of the parameters, in an iterative process are calculated solving the system:

$$[(J^T J + \eta C^T C)]\, \delta p = J^T b \quad (2)$$

where δp is the vector containing the corrections applied to the parameters (logarithm of block conductivities, p_j) of an initial model, b is the vector of the differences between the logarithm of the observed and calculated σ_a [$b_i = \ln(\sigma_a^o/\sigma_a^c)_i$], J is the Jacobian matrix whose elements are given by (σ_j/σ_{ai}^c) $(\partial\sigma_{ai}^c\ \partial\sigma_j)$, the superscript T denotes the transpose operation, and η is a Lagrange multiplier that controls the amplitude of the parameter corrections and whose best value is determined empirically. The elements of matrix C are the coefficients of the values of the roughness of each 1D model, which is defined in terms of the two neighbor's parameters and the constraint between the parameters of the different models on time. In this regard and in our temporal 1D experiment, each cell is constrained spatially by its vertical neighbors, while the temporal constraints are imposed using its lateral neighbors. An iterative process allows the final models to be obtained, with their response fitting the data set in a least-square sense. In terms of η, generally, large values will produce smooth inversion results with smoother spatial and temporal variations.

3.5. Numerical simulation of water flow and chloride transport in soil

The water and the chloride propagation monitored during the experiments were also simulated by using the HYDRUS-1D model (Simunek et al., 1998). HYDRUS-1D simulates water flow and solute transport by solving the Richards equation and the Advection-Dispersion equation, respectively.

Richards equation can be written for one-dimensional, unsaturated, non-steady state flow of water in the vertical direction as follows:

$$C_w(\theta)\frac{\partial h}{\partial t} = \frac{\partial}{\partial z}\left[K(h)\frac{\partial h}{\partial z} + K(h)\right] \quad (3)$$

https://doi.org/10.5194/hess-2022-12
Preprint. Discussion started: 1 February 2022

Hydrology and Earth System Sciences
Open Access
EGU
Discussions

where $C_w(\theta)$, the water capacity, is the slope of the water retention curve, θ is the volumetric water content [L^3L^{-3}], *h* is the soil water pressure head [L], *K*(*h*) is the unsaturated hydraulic conductivity [LT^{-1}].

The Advection-Dispersion equation governing the transport of a single non-reactive and non-adsorbed (a tracer, chloride in our case) ion in the soil can be written as:

$$\frac{\partial(\theta C)}{\partial t} = \frac{\partial}{\partial z}\left[\theta D \frac{\partial C}{\partial z} - qC\right] \quad (4)$$

where *q* is the darcian flux, *C* is the solute concentration in the liquid phase [ML^{-3}], *D* (L^2T^{-1}) is the effective dispersion coefficient, which can be assumed to come from a combination of the molecular diffusion coefficient, D_{diff} (L^2T^{-1}) and the hydrodynamic dispersion coefficient, D_{dis} (L^2T^{-1}):

$$D = D_{diff} + D_{dis} \quad (5)$$

where the hydrodynamic dispersion is the mixing or spreading of the solute during transport due to differences in velocities within a pore and between pores. The dispersion coefficient can be related to the average pore water velocity $v=q/\theta$ through:

$$D = \lambda v \quad (6)$$

where λ [L] is the dispersivity, a characteristic property of the porous medium. To solve the Richards equation (Eq. 3), the water retention function, θ(*h*), and the hydraulic conductivity function, *K*(*h*), must be defined. In this paper we adopted the van Genuchten-Mualem model (vG-M), (Van Genuchten, 1980):

$$S_e = [1 + (\alpha|h|)^n]^{-m} \quad (7)$$

$$K(h) = K_s S_e^{\tau}\left[1 - \left(1 - S_e^{1/m}\right)^m\right]^2 \quad (8)$$

In the Equations 7 and 8, $S_e = \frac{(\theta - \theta_r)}{(\theta_S - \theta_r)}$ is the effective water saturation, θ_s the saturated water content, θ_r the residual water content, α, *n* and *m* are fitting parameters with *m* taken as m=1-1/n, K_s is the saturated hydraulic conductivity and τ is the pore-connectivity parameter.

3.6. Inverse estimation of soil hydraulic and solute transport parameters

The obtained EMI-based spatiotemporal distribution of σ_b during the water infiltration experiment (the 1st experiment) was converted to a θ distribution in order to estimate the temporal evolution of θ during the infiltration process. These water content data were then used in an optimization procedure by using the HYDRUS-1D model, in order to estimate the hydraulic properties of the different horizons in the soil profile. The simulations were carried out by using the actual top boundary flux conditions during the experiment, including the irrigation events. For the bottom boundary, free drainage was considered. A simulation domain 150 cm depth was considered. The same procedure was repeated using the direct measurements of θ (TDR) and pressure head (Tensiometers) in order to obtain independent hydraulic parameters to be compared to those inferred from EMI. A three-layer soil profile (0-25; 25-70; 70-150 cm), reflecting the actual pedological layering (i.e. Ap, Bw, and bedrock) were used in all simulations.

As for the solute transport experiment, a HYDRUS-1D simulation was carried out with the EMI-based hydraulic properties obtained from the 1st experiment to simulate the water content distributions in correspondence with the EMI measurement times. The simulations of water infiltration and solute transport in the 2nd experiment was carried out by using the top boundary fluxes conditions used during the 2nd experiment along with the same simulation domain, three-layer soil profile, and the bottom boundary described above. Thus, for each monitoring time, we

https://doi.org/10.5194/hess-2022-12
Preprint. Discussion started: 1 February 2022

Hydrology and Earth System Sciences Discussions

had available the σ_b distributions obtained from the EMI and θ from the HYDRUS-1D simulations. These distributions allowed us to estimate as many σ_w (and thus *C*) distributions by using the θ-σ_b-σ_w relationship obtained in the laboratory. These *C* distributions were used in a new HYDRUS-1D simulation to estimate the longitudinal dispersivity of the investigated soil. The simulated concentrations, with the optimized dispersivity, were compared to those obtained from the TDR and tensiometer data.

4. RESULTS AND DISCUSSION

4.1. Water infiltration – 1st experiment

4.1.1. Time-lapse σ_a data and estimation of σ_b distribution

Figure 3 shows the σ_a values observed during the water infiltration experiment. Both VCP and HCP modes show a relatively similar pattern of σ_a values with ρ32 and ρ118 being the highest and lowest respectively. HCP mode shows higher values compared to the VCP mode in the same receivers. This pattern of σ_a distribution suggests the presence of a conductive zone over a resistive zone which is expected in this experiment as a result of the waterfront being infiltrated into the soil profile and the presence of a resistive bedrock. In terms of temporal σ_a variabilities, the σ_a increases consistently in both VCP and HCP modes during the first three hours of the experiment. Afterward, σ_a did not change significantly toward the end of the experiment. The range of σ_a variations is relatively small in both VCP and HCP modes with the former in the 10-30 mS m^{-1} range and the latter in the 10-50 mS m^{-1} range.

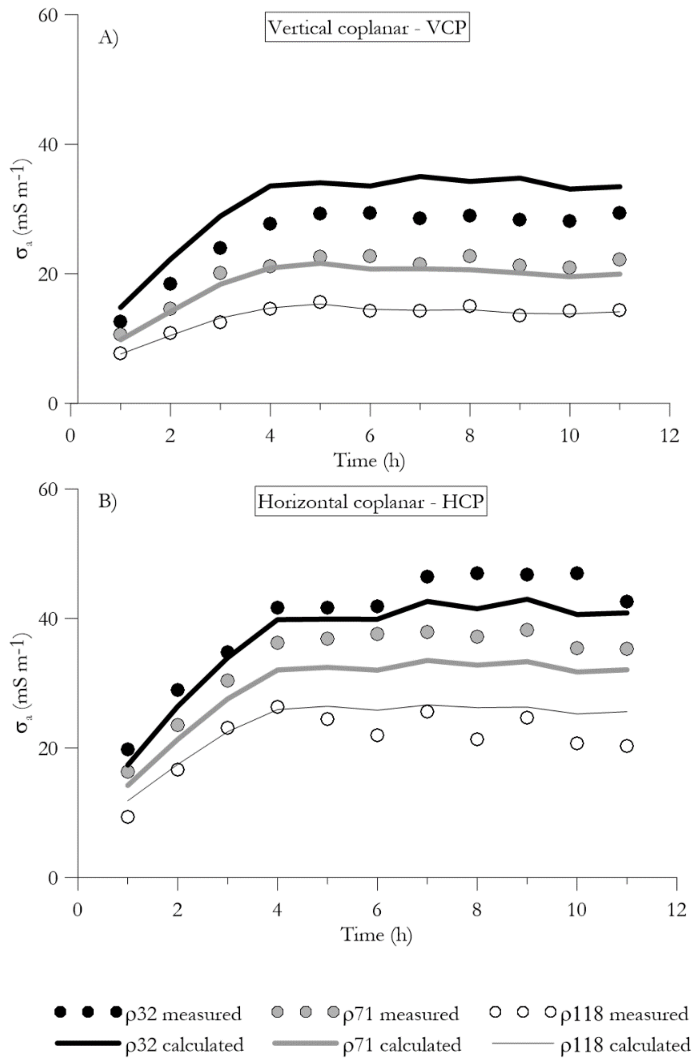

Figure 3: σ_a values observed during the water infiltration experiment. (A) VCP, (B) HCP. The symbols represent the measured data whereas the lines represent the values calculated after the inversion.

321 Fig. 4 depicts the time-lapse σ_b modeling results of σ_a shown in Fig. 3. The model shows clearly
322 the evolution of the conductive zone into the soil profile shortly after the irrigation started as
323 expected from the σ_a data. The resistive zone beneath a conductive zone corresponds to the bedrock

https://doi.org/10.5194/hess-2022-12
Preprint. Discussion started: 1 February 2022

layer in the experimental plot. The σ_b of the resistive zone remains below 5 mS m^{-1} and does not vary significantly during the experiment, while, in contrast, the σ_b of the upper layers increased significantly from an average of 20 mS m^{-1} at the beginning of the experiment to more than 50 mS m^{-1} after the 5th irrigation. The conductivity of this zone does not increase largely since then, suggesting that the soil is fairly saturated after the 3rd irrigation.

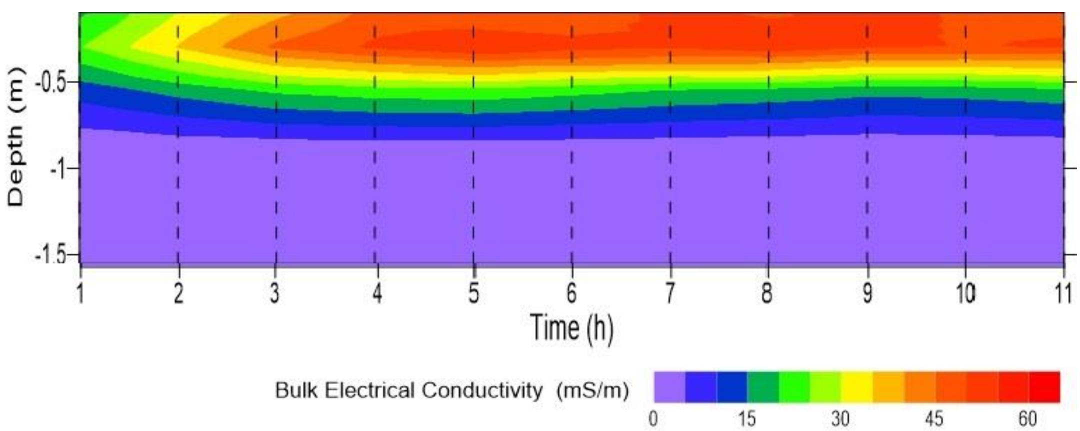

Figure 4. Time evolution of bulk electrical conductivity (σ_b) distribution with depth during the water infiltration experiment.

4.1.2. Comparison between TDR measurements and EMI-based σ_b and θ distribution

Figure 5 shows the temporal σ_b changes inferred from TDR and EMI observations at two depths, 20 and 40 cm, where the TDR probes monitored the water infiltration experiment. As reported by many authors (e.g. Coppola et al., 2016; Dragonetti et al., 2018), both techniques provide σ_b estimations but a direct comparison between σ_b by TDR and EMI is not straightforward due to different volumes of sensor investigation as well as the different nature of measurements. However, this comparison can be used as a means to investigate the consistency of the σ_b trends

https://doi.org/10.5194/hess-2022-12
Preprint. Discussion started: 1 February 2022

and to provide an insight into the uncertainty associated with the EMI survey and inversion process in resolving the water infiltration process into the soil profile. Focusing on the σ_b series inferred from both TDR observations and EMI inversion, a similar time pattern of σ_b variability is evident, but in general, the EMI model underestimates the σ_b obtained by TDR. A better agreement was observed at 20 cm in terms of both absolute σ_b values and trend (*r*=0.94; Mean Error=10.1 mS m^{-1}). In contrast, at 40 cm, the mismatch between TDR observations and EMI inversions becomes larger at the end of the experiment, but still in an acceptable range (*r*=0.54; Mean Error=16.1 mS m^{-1}). The EMI σ_b values – especially at 40 cm depth – remain rather invariant in the last part of the infiltration experiment. The general outcome that for both layers the EMI σ_b values underestimate the TDR σ_b measurements has been frequently found in the literature (e.g. Coppola et al., 2015; Dragonetti et al., 2018; Visconti and De Paz, 2021). von Hebel et al. (2014) also found a similar behavior when comparing their EMI results with ERT surveys. In that case, the σ_a values measured by EMI systematically underestimated the σ_a generated by applying EMI forward modeling to the σ_b distribution retrieved by ERT.

Figure 6 shows the evolution of θ at the same two depths, 20 and 40 cm as observed by TDR and EMI sensors. While TDR provides direct measurements of θ, in order to estimate θ from EMI observation, σ_b values extracted at these depths (Fig. 4) were converted to θ by the calibration performed in the laboratory, as detailed in Farzamian et al., (2021). A rapid increase of θ is visible shortly after injection in both EMI-based and TDR measurements. The EMI-based θ estimation is able to detect the similar water content evolution (similar water content differences over time) observed by direct TDR measurements but at a slightly different water content level. Specifically, EMI water contents were mostly lower than the TDR ones but the two series showed a quasi-

https://doi.org/10.5194/hess-2022-12
Preprint. Discussion started: 1 February 2022

parallel evolution at 20 cm depth (r=0.98; Mean Error=0.09 cm^3 cm^{-3}), while diverging for longer times at 40 cm depth (r=0.60; Mean Error=0.17 cm^3 cm^{-3}).

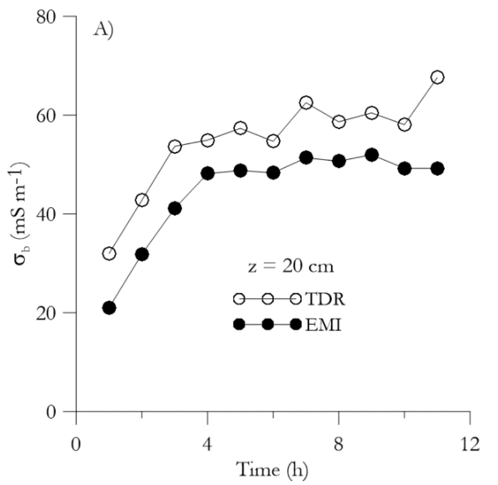

Figure 5. σ_b evolution estimated from the TDR and EMI measurements at 20 cm (A) and 40 cm (B) depths.

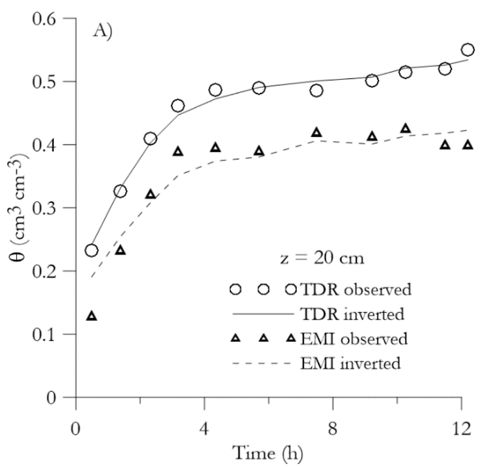

Figure 6. Evolution of θ measured by TDR (circles) and estimated from EMI measurements (triangles) at 20 cm (A) and 40 cm (B) depths. Continuous lines for TDR and dashed lines for EMI refer to the estimation obtained by the inversion procedure of the water infiltration process (see Sect. 4.1.3 below).

https://doi.org/10.5194/hess-2022-12
Preprint. Discussion started: 1 February 2022

Hydrology and Earth System Sciences Discussions

4.1.3. Estimation of hydraulic properties

In order to estimate hydraulic properties parameters, an inversion procedure was performed using the HYDRUS-1D model. The first set of hydraulic parameters was obtained by optimizing soil water content measured by TDR and pressure head measured by tensiometers (hereafter TDR-based for sake of simplicity). The second set of hydraulic parameters was obtained by optimizing soil water content estimated by EMI measurements (hereafter EMI-based). The inversion simulations were carried out by fixing θ_r=0 and τ=0.5, while θ_s, α, n and K_s were optimized for all the layers considered. The hydraulic properties of the bedrock were fixed to θ_r=0.068, θ_s=0.354, α=0.055, n=3.67, τ=0.5 and k_s=19.02 according to Caputo et al. (2010; 2015).

Figure 6 reports a comparison between water contents measured (symbols) and estimated (lines) by the inversion procedure. The θ distribution was properly estimated at 20 cm depth in both approaches. However, a lower agreement was obtained at 40 cm but still acceptable. Table 1 reports the parameters of the hydraulic functions, estimated for the first two horizons. Figure 7 reports the water retention curves and the hydraulic conductivity curves corresponding to the parameters shown in table 1 for a better comparison between TDR-based and EMI-based hydraulic properties assessment.

As for water retention, the TDR and EMI water retention curves showed similar shapes but with slightly different saturated water contents. As discussed earlier, the slightly lower saturated water content is not surprising for the EMI-based estimation due to the overall underestimation of water content. The two curves almost overlapped once scaling the EMI curve by the ratio of the saturated water contents. Obviously, this result is consistent with the underestimation of EMI-based θ distributions as shown in Fig. 6.

https://doi.org/10.5194/hess-2022-12
Preprint. Discussion started: 1 February 2022

Hydrology and Earth System Sciences Discussions

As for the hydraulic conductivity, TDR-based and EMI-based hydraulic conductivity curves at both 20 and 40 cm appear to almost overlap, with similar saturated hydraulic conductivity and curve shape. This result is expected because the hydraulic conductivity is mainly a function of the variation of θ and not the absolute value of θ itself. It is worth mentioning that the same top boundary flux and different water contents in the soil profile provided similar EMI-based and TDR-based hydraulic conductivity. These conditions lead to two different water flow processes, with simulations predicting higher water stored in the soil profile and lower downward fluxes (data not shown) when TDR-based results are compared to the EMI-based results.

Table 1. vG-M Hydraulic parameters (Eqs. 7 and 8) and dispersivity, λ (Eq. 6) for Ap and Bw horizons

Soil hydraulic and transport parameters		Ap		Bw	
		TDR-based	EMI-based	TDR-based	EMI-based
θ_r	[cm^3 cm^{-3}]	0.00	0.00	0.00	0.00
θ_s	[cm^3 cm^{-3}]	0.54	0.45	0.52	0.45
α	[cm^{-1}]	0.006	0.003	0.009	0.007
n	[-]	1.70	1.54	1.50	1.41
k_s	[cm min^{-1}]	0.06	0.02	0.28	0.29
τ	[-]	0.5	0.5	0.5	0.5
λ	[cm]	10	12	0.5	0.8

https://doi.org/10.5194/hess-2022-12
Preprint. Discussion started: 1 February 2022

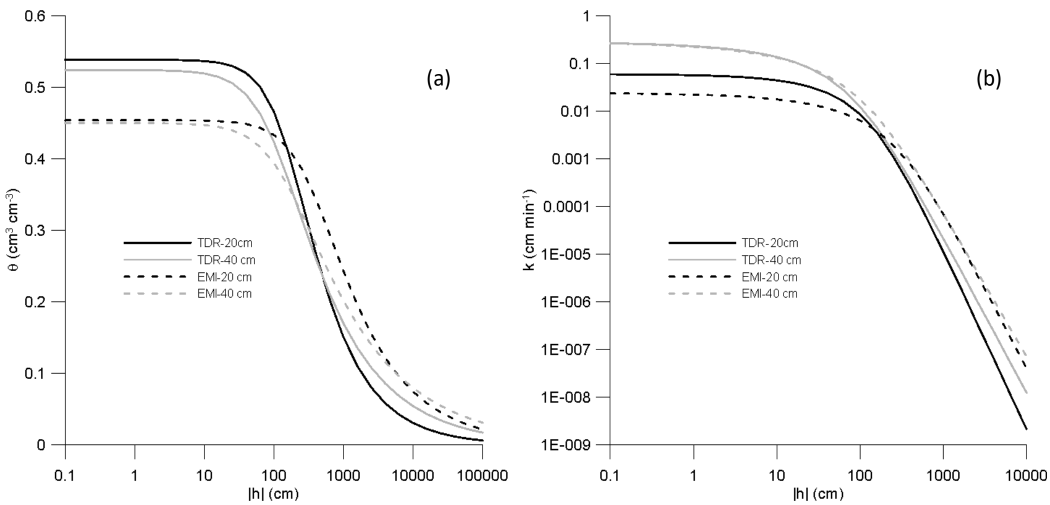

Figure 7. Soil water retention (A) and unsaturated hydraulic conductivity (B) curves, estimated from the TDR and EMI measurements at 20 cm and 40 cm depths.

4.2. Solute Infiltration – 2nd Experiment

4.2.1. Time-lapse σ_a data and estimation of σ_b distribution

Figure 8 shows the σ_a data collected during the solute infiltration experiment. Again, as for the water infiltration experiment, both VCP and HCP modes show a relatively similar pattern of σ_a values with ρ32 and ρ118 being the highest and lowest respectively. HCP mode shows higher values on average compared to the VCP mode. Similarly, to the water infiltration experiment, σ_a increases consistently during the first three hours of the experiment, then it does not change significantly or consistently until the end of the experiment. Much higher ranges of σ_a variations were measured in both VCP and HCP configurations, with σ_a values ranging in 20-200 and 50-250 mS m^{-1} respectively.

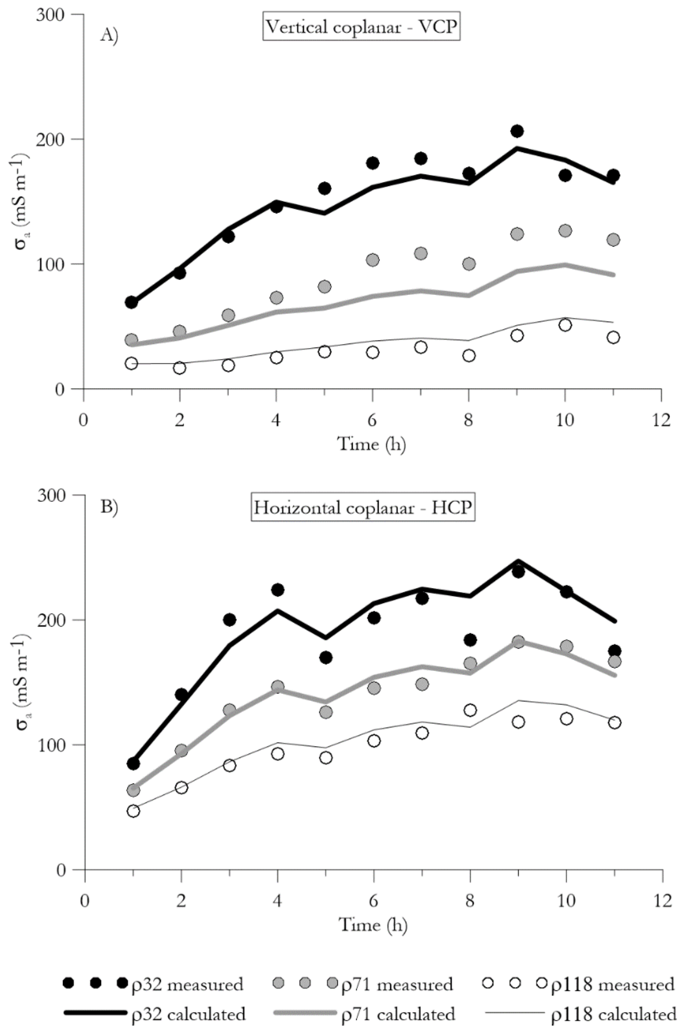

Figure 8: σ_a values observed during the solute infiltration experiment. (A) VCP, (B) HCP. The symbols represent the measured data whereas the lines represent the values calculated after the inversion.

Figure 9 depicts the σ_b evolution for the solute infiltration experiment, obtained by time-lapse inversion of σ_a data. The results show the rapid evolution of the conductive zone to the soil profile shortly after the irrigation started. In comparison to the obtained σ_b in the 1st experiment, the results

https://doi.org/10.5194/hess-2022-12
Preprint. Discussion started: 1 February 2022

reveal significantly higher soil conductivity in topsoil but a much slower evolution. The conductivity of the top layer exceeds 300 mS m^{-1} shortly after the irrigation. The higher topsoil conductivity results from injection of high-saline water (about 15 dS m-1) that dramatically increases soil conductivity whereas the smaller evolution of the conductive zone is caused by significantly slower concentration propagation into the soil profile.

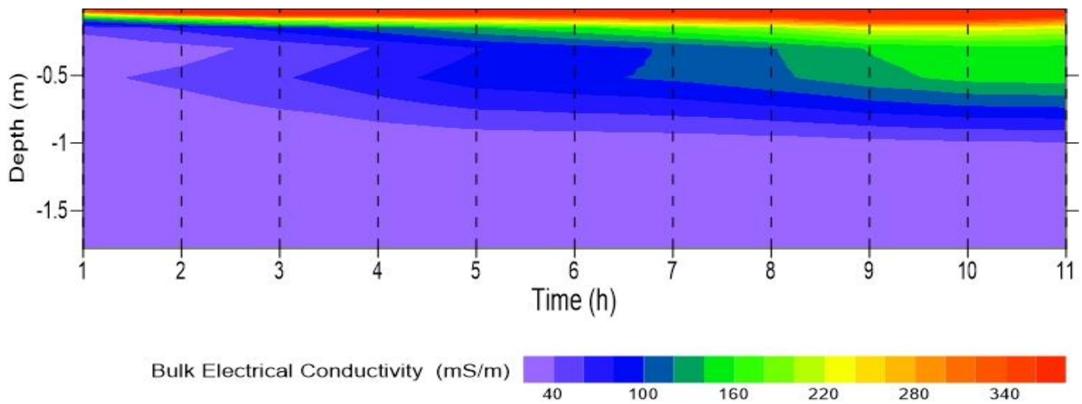

Figure 9. Time evolution of bulk electrical conductivity (σ_b) during the solute infiltration experiment.

4.2.2. Comparison between TDR measurements and EMI-based σ_b and [Cl^-] distribution

Figure 10 shows the comparison between the σ_b values obtained by the TDR measurements and those obtained from the EMI inversion (Fig. 9) during the 2nd experiment. As discussed above, this comparison is to provide an insight into the potential of the EMI survey and inversion process in monitoring a solute transport experiment into a soil profile. The comparison shows a similar time pattern of σ_b variability, but in general, the EMI model slightly underestimates the σ_b obtained by TDR. The results of this comparison agree with the 1st experiment where, again, the EMI-based

σ_b are lower compared to those measured by the TDR. In contrast to the 1st experiment, the differences between the two techniques and in terms of the absolute σ_b values are of minor concern. This is expected to be due to the larger conductivity contrast that tracer introduced into the soil profile in the 2nd experiment which became easier to detect by using the EMI sensor. On the other hand, the TDR probes show more fluctuations in σ_b measurements, especially at 20 cm. We attribute these fluctuations to the smaller volume of investigation of the TDR probes which are very sensitive to the process taking place very close to the probe and, therefore, strongly influenced by small-scale local variability.

The next step in the procedure allows us to determine the distribution of Cl^- concentrations by both TDR and EMI sensors. TDR-based Cl^- distributions were obtained directly in the field from a direct measurement of the impedance Z along the TDR transmission line embedded in the soil. As for the EMI-based Cl^- concentrations, a forward HYDRUS-1D simulation was carried out using the EMI-based hydraulic properties obtained from the 1st experiment and reported in Table. 1 to estimate the water content distributions in correspondence with the EMI measurement times of the 2nd experiment. These water contents, combined with the available σ_b distribution obtained from the EMI inversion, allowed us to obtain the σ_w distributions (through the θ-σ_b-σ_w calibration relationship) for both depths and, consequently, the Cl^- distributions. Finally, the latter was used again for estimating the longitudinal dispersivity of the two soil layers investigated (Sect. 4.2.3.).

https://doi.org/10.5194/hess-2022-12
Preprint. Discussion started: 1 February 2022

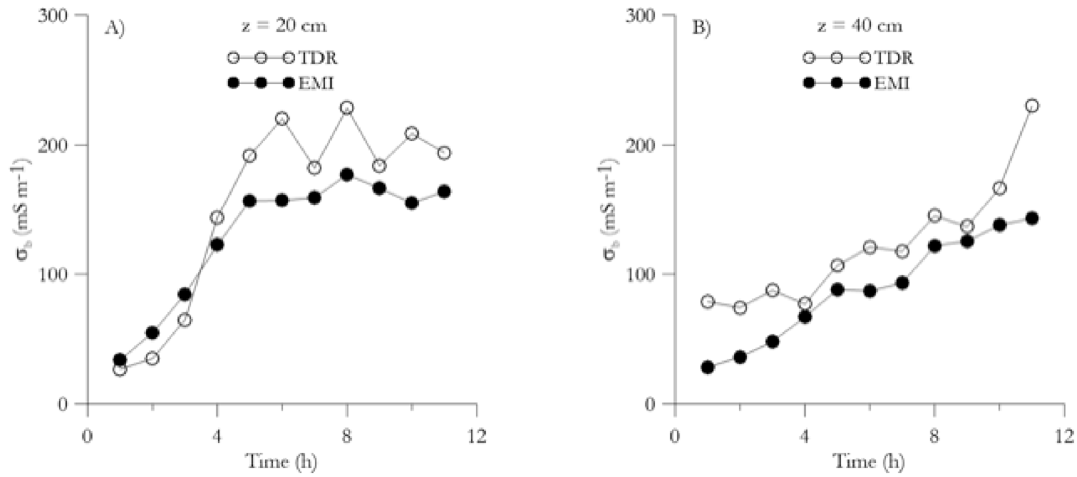

Figure 10. σ_b evolution estimated by TDR and EMI measurements at 20 cm (a) and 40 cm (b) depth.

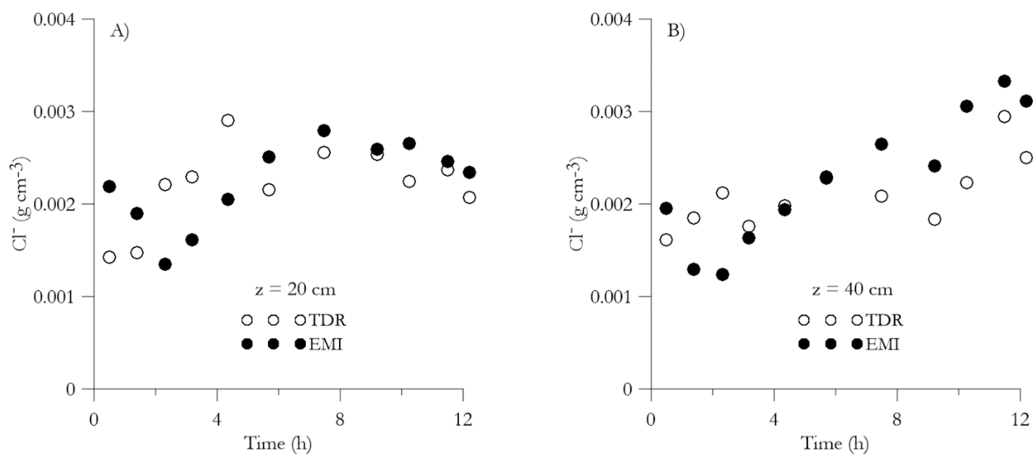

Figure 11. Cl^- distributions inferred from EMI and TDR measurements.

Figure 11 shows the Cl^- distributions inferred from EMI compared to the TDR measurements. The comparison suggests a good agreement between the two time series. The EMI-based concentrations underestimate the TDR-based ones by 4% and by 7% at 20 cm and 40 cm depths, respectively. The time evolution of the two data series reveals marked differences, as shown by the very different correlation: r = - 0.04 for the 20 cm depth and r = 0.70 for the 40 cm depth. The difference between the two data series at both depths can be mostly explained by the differences between σ_b distributions shown in Fig. 10. Additionally, another point of difference may arise from the assumption that the water content distribution obtained from the HYDRUS-1D simulation can be used as a substitute for the water content measurements, in order to obtain [Cl-] from the EMI readings. However, this is different compared to the direct measurements of TDR in the 2nd experiment and therefore introduces more mismatch between [Cl^-] plots.

4.2.3. Estimation of longitudinal dispersivity

Inverse HYDRUS-1D simulations were conducted using concentration data provided by both the TDR and EMI results, in order to estimate the longitudinal dispersivity λ for both Ap and Bw horizons. The results are reported in Table 1. TDR-based and EMI-based procedures provide similar values of λ. Specifically, for the Ap horizon, the obtained values agree with those frequently found in the literature for either large columns or field-measured dispersivity (e.g., Vanderborght and Vereecken, 2007; Coppola et al., 2011b). The TDR and EMI-based estimation of dispersivity for the Bw horizon shows one order of magnitude lower values compared to the Ap horizon. These values are more consistent with values measured in the laboratory (Coppola et al., 2009).

https://doi.org/10.5194/hess-2022-12
Preprint. Discussion started: 1 February 2022

5. Conclusion and outlook

In this study, we carried out two sequential water infiltration and solute transport experiments and conducted time-lapse EMI surveys to examine how well this methodology can be used to i) monitor water content dynamic after irrigation and to estimate the soil hydraulic van Genuchten–Mualem parameters from the first experiment and ii) to monitor solute concentration, C, and to assess solute dispersivity. We then compared the obtained results to those estimated by direct TDR and tensiometer probes measurements. Based on our study, the following main conclusions can be drawn:

1. The EMI-based estimation of θ can detect the similar water content evolution in time when compared to direct TDR measurements in the 1st experiment, however, a significant underestimation was observed in the EMI-based estimation of θ. This is expected when we compare σ_b evolution from the inversion of σ_a data with the TDR-based σ_b measurements. With regard to the 2nd experiment, a similar time pattern of σ_b variability can also be seen between the two approaches. However, the differences between the two approaches are of minor concern in both σ_b distribution and [Cl^-]. We attribute the smaller underestimation of σ_b distribution and [Cl^-] in the 2nd experiment to the larger conductivity contrast that tracer introduced into the soil profile in the 2nd experiment which became easier to detect by using the EMI sensor.
2. The proposed methodology for the estimation of vG-M parameters proved to be effective for both Ap and Bw horizons. The overall EMI-based underestimation of θ did not impact the hydraulic conductivity curves significantly as the hydraulic conductivity is the main function of the variation of θ. On the other hand, this underestimation resulted in lower saturated

https://doi.org/10.5194/hess-2022-12
Preprint. Discussion started: 1 February 2022

water content which also appeared in the water retention curve. The overall approach shows the high potential of the EMI sensor to replace TDR and tensiometer probes in the field-scale assessment of soil hydraulic properties. In practice, one could monitor a relatively short infiltration experiment with an EMI sensor and use the water content estimations in an inversion procedure to estimate the hydraulic properties. The latter can be simply converted to more accurate water content distribution by direct measurement of the actual saturated water content at the end of the experiment using TDR probes or even by taking samples and laboratory measurements.

3. In terms of the longitudinal dispersivity, λ, there was a very good agreement between EMI-based and TDR-based estimation for both Ap and Bw horizons. The finding results are also in very good agreement with previous in-situ and laboratory measurements which suggests that the proposed methodology can be used in the field-scale assessment of the longitudinal dispersivity, λ which is indeed an important parameter in soil salinity simulations in salt-affected regions across the world. However, this method requires that the hydraulic properties of the investigated soil at the scale of concern be assessed prior to the application of this method to discriminate the contribution of water content and concentration in the EMI-based σ_b estimation.

4. The application of EMI for detailed investigation of the infiltration process has several limitations apart from the overall underestimation of water content and concentration and requires further investigation. Resolving the wetting zone during the water injection is one source of uncertainty in this approach. The water content sharply decreases with depth in this zone to near the initial water content of the soil and causes dramatic resistivity variation. In addition, a very shallow resistive bedrock exists in the study site which added to the

https://doi.org/10.5194/hess-2022-12
Preprint. Discussion started: 1 February 2022

complexity of resolving three zones with very different resistivity. The limited number of σ_a measurements (total of 6) is not sufficient for recovering the sharp σ_b variability that takes place during the infiltration. In addition, a smoothness constraint was performed in the inversion process to stabilize the inversion process which further smooths the layer boundaries in this approach. Measuring σ_a at different heights enables us to collect more σ_a data to better resolve changes that occur over short depth increments. More importantly, the application of a coupled Hydro-Geophysical approach (e.g. Hinnell et al. 2010; Huisman et al. 2010) can improve the estimation of the parameters by considering all of the hydrologic and geophysical data in a single inversion. In the coupled approach, geophysical data are not inverted individually and a regularization/smoothness constraint is no longer required to stabilize the geophysical component of the inverse problem.

5. Water irrigation and soil salinity management and thus hydrological investigations are usually large-scale challenges. The EM method is a non-invasive, fast, and cost-effective technique, covering large areas in less time and at a lower cost. Our study reveals the potential of this method for hydrological studies on large scales. However, our study was limited to a controlled experiment on a plot scale. More investigations have to be conducted in this area to evaluate the potential of EMI sensors under different soil conditions and within the larger 2D and 3D investigations to further address the limitations of this methodology at desired field scale. Our study also shows that we cannot use geophysical imaging alone and we need to use other in-situ data to support Hydro-Geophysical approach. Last but not least, proper estimation of soil hydraulic and hydrodispersive properties relies on an appropriate understanding of both geophysical and hydrogeological data and modeling approaches and requires close collaboration of geophysicists and hydrologists.

ACKNOWLEDGMENTS

This work was funded in the scope of the project SALTFREE: Salinization in irrigated areas: risk evaluation and prevention [ARIMNet2, Grant agreement no. 618127], by the Italian Ministry of Agricultural, Food and Forestry Policies [D.M. 28675/7303/15]. M. Farzamian was supported by a contract within project SOIL4EVER [Increasing water productivity through the sustainable use of soils, PTDC/ASP-SOL/28796/2017].

REFERENCES

Abbasi, F., Simunek, J., Feyen, J., van Genuchten, M.T., and Shouse, P.T.: Simultaneous inverse estimation of soil hydraulic and solute transport parameters from transient field experiments: Homogeneous soil. Transactions of the ASAE 46(4): 1085, 2003.

Archie, G.E.: The electrical resistivity log as an aid in determining some reservoir characteristics. Transactions of the AIME 146(01): 54–62, 1942.

Basile, A., Ciollaro, G., and Coppola, A.: Hysteresis in soil water characteristics as a key to interpreting comparisons of laboratory and field measured hydraulic properties, Water Resour. Res., 39, 1–12, https://doi.org/10.1029/2003WR002432, 2003.

Basile, A., Coppola, A., De Mascellis, R., and Randazzo, L.: Scaling Approach to Deduce Field Unsaturated Hydraulic Properties and Behavior from Laboratory Measurements on Small Cores, Vadose Zone J., 5, 1005–1016, https://doi.org/10.2136/vzj2005.0128, 2006.

Binley, A., Cassiani, G., Middleton, R., and Winship, P.: Vadose zone flow model parameterisation using cross-borehole radar and resistivity imaging. Journal of Hydrology 267(3–4): 147–159, https://doi.org/10.1016/S0022-1694(02)00146-4, 2002.

Bouksila, F., Persson, M., Bahri, A., and Berndtsson, A.: Electromagnetic induction prediction of soil salinity and groundwater properties in a Tunisian Saharan oasis. Hydrological sciences journal 57(7): 1473–1486, https://doi.org/10.1080/02626667.2012.717701. 2012.

Caputo, M.C., De Carlo, L., Masciopinto, C., and Nimmo, J.R.: Measurement of field-saturated hydraulic conductivity on fractured rock outcrops near Altamura (Southern Italy) with an adjustable large ring infiltrometer, Environ. Earth Sci., 60, 583–590, https://doi.org/10.1007/s12665-009-0198-y, 2010.

Caputo M.C., Maggi S., and Turturro A.C.: Calculation of Water Retention Curves of Rock Samples by Differential Evolution, in: Engineering Geology for Society and Territory, edited by Lollino G., Manconi A., Guzzetti F., Culshaw M., Bobrowsky P., Luino F. (eds), Volume 5, Springer, Cham, https://doi.org/10.1007/978-3-319-09048-1, 2015.

Chaali, N., Comegna, A., Dragonetti, G., Todorovic, M., Albrizio, R., Lamaddalena, N., and Coppola, A.: Monitoring and modeling root-uptake salinity reduction factors of a tomato crop under non-uniform soil salinity distribution. Procedia Environmental Sciences. vol. 19, p. 643-653, 2013.

Comegna, V., Coppola, A., Basile, A., and Comegna, A.: Review of Approaches for Measuring Soil Hydraulic Properties and Assessing the Impacts of Spatial Dependence on the Results. In: G. A. Kazemi. Hydrogeology a Global Perspective. InTech, ISBN: 9789535100485, 2012.

Coppola, A., Comegna, A., Dragonetti, G., Lamaddalena, N., Kader, A. M., and Comegna, V.: Average moisture saturation effects on temporal stability of soil water spatial distribution at field scale, Soil Till. Res., 114, 155–164, https://doi.org/10.1016/j.still.2011.04.009, 2011a.

Coppola, A., Comegna, A., Dragonetti, G., Dyck, M., Basile, A., Lamaddalena, N., Kassab, M., and Comegna, V.: Solute transport scales in an unsaturated stony soil, Adv. Water Resour., 34, 747–759, https://doi.org/10.1016/j.advwatres.2011.03.006, 2011b.

Coppola, A., Smettem, K., Ajeel, A., Saeed, A., Dragonetti, G., Comegna, A., Lamaddalena, N., and Vacca, A.: Calibration of an electromagnetic induction sensor with time-domain reflectometry data to monitor rootzone electrical conductivity under saline water irrigation, Eur. J. Soil Sci., 67, 737–748, https://doi.org/10.1111/ejss.12390, 2016.

Coppola, A., Dragonetti, G., Comegna, A., Lamaddalena, N., Caushi, B., Haikal, M. A., and Basile, A.: Measuring and modeling water content in stony soils, Soil Till. Res., 128, 9–22, https://doi.org/10.1016/j.still.2012.10.006, 2013.

Coppola, A., Dragonetti, G., Sengouga, A., Lamaddalena, N., Comegna, A.: Identifying Optimal Irrigation Water Needs at District Scale by Using a Physically Based Agro-Hydrological Model. Water 11(4). https://doi.org/10.3390/w11040841, 2019.

Coppola, A., Chaali, N., Dragonetti, G., Lamaddalena, N., and Comegna, A.: Root uptake under non-uniform root-zone salinity, Ecohydrology, 8, 1363–1379, https://doi.org/10.1002/eco.1594, 2015.

Corwin, D. L., and Lesch, S. M.: Apparent soil electrical conductivity measurements in agriculture, Comput. Electron. Agr., 46, 11–43, https://doi.org/10.1016/j.compag.2004.10.005, 2005.

Dragonetti, G., Comegna, A., Ajeel, A., Deidda, G. P., Lamaddalena, N., Rodriguez, G., Vignoli, G., and Coppola, A.: Calibrating electromagnetic induction conductivities with time-domain reflectometry measurements, Hydrol. Earth Syst. Sci., 22, 1509–1523, https://doi.org/10.5194/hess-22-1509-2018, 2018.

Ellsworth, T.R., Shaouse, P.J., Jobes, J.A., Fargerlund, J., and Skaggs, T.H.: Solute transport in unsaturated soil: Experimental design, parameter estimation, and model discrimination. Soil Science Society of America Journal 60(2): 397–407, https://doi.org/10.2136/sssaj1996.03615995006000020010x, 1996.

Farzamian, M., Monteiro Santos, F. A., and Khalil, M. A.: Application of EM38 and ERT methods in estimation of saturated hydraulic conductivity in unsaturated soil, J. Appl. Geophys., 112, 175–189, https://doi.org/10.1016/j.jappgeo.2014.11.016, 2015a.

Farzamian, M., Monteiro Santos, F. A., and Khalil, M. A.: Estimation of unsaturated hydraulic parameters in sandstone using electrical resistivity tomography under a water injection test, J. Appl. Geophys., 121, 71–83, https://doi.org/10.1016/j.jappgeo.2015.07.014, 2015b.

Farzamian, M., Monteiro Santos, F. A., Khalil, A.M.: Constraining Unsaturated Hydraulic Parameters Using the Latin Hypercube Sampling Method and Coupled Hydrogeophysical Approach. Pure Appl. Geophys. https://doi.org/10.1007/s00024-017-1656-1, 2017.

Farzamian, M., Ribeiro, J.A., Monteiro Santos, F.A., Khalil M.A.: Application of Transient Electromagnetic and Audio-Magnetotelluric Methods for Imaging the Monte Real Aquifer in Portugal. Pure Appl. Geophys, https://doi.org/10.1007/s00024-018-2030-7, 2019.

Farzamian, M., Paz, M. C., Paz, A. M., Castanheira, N. L., Gonçalves, M. C., Monteiro Santos, F. A., and Triantafilis, J.: Mapping soil salinity using electromagnetic conductivity imaging–A comparison of regional and location-specific calibrations, Land. Degrad. Dev., 30, 1393–1406, https://doi.org/10.1002/ldr.3317, 2019.

Farzamian, M., Vieira, G., Monteiro Santos, F. A., Yaghoobi Tabar, B., Hauck, C., Paz, M. C., Bernando, I., Ramos, M., de Pablo, M. A.: Detailed detection of active layer freeze–thaw dynamics using quasi-continuous electrical resistivity tomography (Deception Island, Antarctica), The Cryosphere, 14, 1105–1120, https://doi.org/10.5194/tc-14-1105-2020, 2020.

Farzamian, M., Autovino, D., Basile, A., De Mascellis, R., Dragonetti, G., Monteiro Santos, F., Binley, A., and Coppola, A.: Assessing the dynamics of soil salinity with time-lapse inversion of electromagnetic data guided by hydrological modelling, Hydrol. Earth Syst.

Sci., 25, 1509–1527, https://doi.org/10.5194/hess-25-1509-2021, 2021.

Groh, J., Stumpp, C., Lücke, A., Pütz, T., Vanderborght, J., Vereecken, H.: Inverse estimation of soil hydraulic and transport parameters of layered soils from water stable isotope and lysimeter data. Vadose Zone Journal 17(1): 1–19, https://doi.org/10.2136/vzj2017.09.0168, 2018.

Hinnell, A.C., Ferre, T.P.A., Vrugt, J.A., Huisman, J.A., Moysey, S., Rings, J., and Kowalsky, M.B.: Improved extraction of hydrologic information from geophysical data through coupled hydrogeophysical inversion. J. Water Resour. Res. 46, W00D40, https://doi.org/10.1029/2008WR007060, 2010.

Huang, J., Monteiro Santos, F. A., and Triantafilis, J.: Mapping soil water dynamics and a moving wetting front by spatiotemporal inversion of electromagnetic induction data, Water Resour. Res., 52, 9131–9145, https://doi.org/10.1002/2016WR019330, 2016.

Huisman, J.A., Rings, J., Vrugt, J.A., Sorg, J., and Vereecken H.: Hydraulic properties of a model dike from coupled Bayesian and multi-criteria hydrogeophysical inversion. J. Hydrol. 380, 62–73, https://doi.org/10.1016/j.jhydrol.2009.10.023, 2010.

Inoue, M., Šimuunek, J., Shiozawa, S., and Hopmans, J.W.: Simultaneous estimation of soil hydraulic and solute transport parameters from transient infiltration experiments. Advances in Water Resources 23(7): 677–688, https://doi.org/10.1016/S0309-1708(00)00011-7, 2000.

Kaufman, A.A., and Keller, G.V.: Frequency and Transient Sounding Methods Geochemistry and Geophysics. Elsevier Science Ltd, New york, 1983.

Kemna, A., Vanderborght, J., Kulessa, B., and Vereecken, H.: Imaging and characterization of subsurface solute transport using electrical resistivity tomography (ERT) and equivalent transport models. Journal of hydrology 267(3–4): 125–146, https://doi.org/10.1016/S0022-1694(02)00145-2, 2002.

Koganti, T., Narjary, B., Zare, E., Pathan, A.L., Huang, J., and Triantafilis, J.: Quantitative mapping of soil salinity using the DUALEM-21S instrument and EM inversion software, Land Degradation and Development, vol. 29, pp. 1768 - 1781, http://dx.doi.org/10.1002/ldr.2973, 2018.

Malicki, M. A. and Walczak, R. T.: Evaluating soil salinity status from bulk electrical conductivity and permittivity, Eur. J. Soil Sci., 50, 505–514, https://doi.org/10.1046/j.1365-2389.1999.00245.x, 1999.

McLachlan, P., Blanchy, G., and Binley, A.: EMagPy: Open-source standalone software for processing, forward modeling and inversion of electromagnetic induction data.

Computers & Geosciences. https://doi.org/10.1016/j.cageo.2020.104561, 2020.

Moghadas, D.: Probabilistic Inversion of Multiconfiguration Electromagnetic Induction Data Using Dimensionality Reduction Technique: A Numerical Study, Vadose Zone J., 18, 1–16, https://doi.org/10.2136/vzj2018.09.0183, 2019.

Monteiro Santos, F. A.: 1D laterally constrained inversion of EM34 profiling data, J. Appl. Geophys., 56, 123–134, https://doi.org/10.1016/j.jappgeo.2004.04.005, 2004.

Paz, A. M., Castanheira, N., Farzamian, M., Paz, M. C., Gonçalves, M. C., Monteiro Santos, F. A., and Triantafilis, J.: Prediction of soil salinity and sodicity using electromagnetic conductivity imaging, Geoderma, 361, 114086, https://doi.org/10.1016/j.geoderma.2019.114086, 2020a.

Paz, M. C., Farzamian, M., Paz, A. M., Castanheira, N. L., Gonçalves, M. C., and Monteiro Santos, F.: Assessing soil salinity using time-lapse electromagnetic conductivity imaging, SOIL, 6, 499–511, https://doi.org/10.5194/soil-6-499-2020, 2020b.

Paz, M. C., Farzamian, M., Santos, F. M., Gonçalves, M. C., Paz, A. M., Castanheira, N. L., and Triantafilis, J.: Potential to map soil salinity using inversion modelling of EM38 sensor data, First Break, 37, 35–39, https://doi.org/10.3997/1365-2397.2019019, 2019.

Robinson, D.A., Jones, S.B., Wraith, J.M., Or, D., and Friedman, S.P..: A Review of Advances in Dielectric and Electrical Conductivity Measurement in Soils Using Time Domain Reflectometry. Vadose Zone Journal 2: 444–475. doi: 10.2136/vzj2003.4440, 2003.

Saeed A., Comegna, A., Dragonetti, G., Lamaddalena, N., Coppola, A.: Soil surface electrical conductivity estimated by TDR and EMI sensors: Accounting for the different sensor observation volumes, J. of Agricultural Engineering. Vol XLVIII, doi:10.4081/jae.2017.716, 2017.

Sasaki, Y.: Full 3-D inversion of electromagnetic data on PC. Journal of Applied Geophysics 46(1): 45–54. doi: 10.1016/S0926-9851(00)00038-0, 2001.

Severino G, Comegna A., Coppola A., Sommella A., Santini A.: Stochastic analysis of a field-scale unsaturated transport experiment, Advances in Water Resources, doi:10.1016/j.advwatres.2010.09.004, 2010.

Šimůnek, J., Angulo-Jaramillo, R., Schaap, M.G., Vandervaere, J.P., and van Genuchten, M.T.: Using an inverse method to estimate the hydraulic properties of crusted soils from tension-disc infiltrometer data. Geoderma 86(1): 61–81. doi: 10.1016/S0016-7061(98)00035-4, 1998.

Simunek, J., Sejna, M., Van Genuchten, M.T., Šimuunek, J., and Šejna, M.: HYDRUS-1D.

Simulating the one-dimensional movement of water, heat, and multiple solutes in variably-saturated media, version 2, 1998.

Singha, K., and Gorelick. S.M.: Saline tracer visualized with three-dimensional electrical resistivity tomography: Field-scale spatial moment analysis. Water Resources Research 41(5). https://doi.org/10.1029/2004WR003460, 2005.

Sposito, G.: Scale Dependence and Scale Invariance in Hydrology, Cambridge Univ. Press, New York, https://doi.org/10.1017/CBO9780511551864, 1999.

Vanderborght J., and Vereecken, H.: Review of Dispersivities for Transport Modeling in Soils. Vadose Zone Journal 6(1) doi:10.2136/vzj2006.0096, 2007.

van Genuchten, M. T.: A closed-form equation for predicting the hydraulic conductivity of unsaturated soils, Soil Sci. Soc. Am. J., 44, 892–898, 1980.

van Genuchten, M.T., Leij, F.J. and Wu, L.: Characterization and measurement of the hydraulic properties of unsaturated porous media (parts 1 and 2). Proceedings of the International Workshop, Riverside, Calif., 22--24 Oct, 1999.

Visconti, F., and de-Paz, J. M.: Sensitivity of soil electromagnetic induction measurements to salinity, water content, clay, organic matter and bulk density. Precision Agriculture, 2021,1-19, doi: 10.1007/s11119-021-09798-8, 2021.

von Hebel, C., Rudolph, S., Mester, A., Huisman, J. A., Kumbhar, P., Vereecken, H., and van der Kruk, J.: Three-dimensional imaging of subsurface structural patterns using quantitative large-scale multiconfiguration electromagnetic induction data, Water Resour. Res., 50, 2732–2748, https://doi.org/10.1002/2013WR014864, 2014.

Wang, X.-p., Quan, G.-j., Pan, Y.-x., Hu, R., Zhang, Y.-f., Tedeschi, A., Basile, A., Comegna, A., Coppola, A. and de Mascellis, R.: 2013. Comparison of hydraulic behavior of unvegetated and vegetation-stabilized sand dunes in arid desert ecosystems. Ecohydrol., 6: 264–274, 2013.

Wessolek, G., Plagge, R. Leij, F.J., and Van Genuchten, M.T..: Analysing problems in describing field and laboratory measured soil hydraulic properties. Geoderma 64(1–2): 93–110. https://doi.org/10.1016/0016-7061(94)90091-4, 1994.

Whalley, W. R., Binley, A. M., Watts, C. W., Shanahan, P., Dodd, I. C., Ober, E. S., Ashton, R. W., Webster, C. P., White, R. P., and Hawkesford, M. J.: Methods to estimate changes in soil water for phenotyping root activity in the field, Plant Soil, 415, 407–422. https://doi.org/10.1007/s11104-016-3161-1, 2017.

Zare, E., Li, N., Khongnawang, T., Farzamian, M., and Triantafilis, J.: Identifying Potential Leakage Zones in an Irrigation Supply Channel by Mapping Soil Properties Using

https://doi.org/10.5194/hess-2022-12
Preprint. Discussion started: 1 February 2022

Electromagnetic Induction, Inversion Modelling and a Support Vector Machine, Soil Syst., 4, 25, https://doi.org/10.3390/soilsystems4020025, 2020.

Zech, A., Attinger, S., Cvetkovic, V., Dagan, G., P. Dietrich, Fiori, A., Rubin, Y., Teutsch, G.: Is unique scaling of aquifer macrodispersivity supported by field data? Water resources research 51(9): 7662–7679, https://doi.org/10.1002/2015WR017220, 2015.